Original Paper

A novel NMR methodology for the quantitative characterization of solid organic matter in shale oil

Chen-Yu Xu [a,b], Ran-Hong Xie [a,b,*], Jiang-Feng Guo [a,b], Xiang-Yu Wang [a,b], Li-Zhi Xiao [a,b], Guo-Wen Jin [a,b], Bo-Chuan Jin [a,b], Xiao-Long Ju [a,b]

[a] State Key Laboratory of Petroleum Resources and Engineering, China University of Petroleum (Beijing), Beijing, 102249, China
[b] Key Laboratory of Earth Prospecting and Information Technology, China University of Petroleum (Beijing), Beijing, 102249, China

ARTICLE INFO

Article history:
Received 22 June 2025
Received in revised form
24 August 2025
Accepted 4 November 2025
Available online 8 November 2025

Edited by Meng-Jiao Zhou

Keywords:
Shale oil reservoir
Solid organic matter
Nuclear magnetic resonance
Free induction decay
T_1-T_2^* spectra

ABSTRACT

Continental shale oil reservoirs in China, particularly those of low to medium maturity, contain a high proportion of untransformed solid organic matter (SOM). The SOM plays a critical role as a potential oil and gas resource. Nuclear magnetic resonance (NMR) is a powerful technique for the evaluation of shale oil reservoirs. However, it is challenging for conventional T_1-T_2 measurement methods to fully capture signals from ultra-short relaxation components such as SOM, due to the measurement deficiency caused by NMR instruments. To this end, the free induction decay (FID) and inversion recovery FID (IR-FID) pulse sequences are introduced, and two novel methods are proposed for quantitative characterization of SOM. The first method, Method I, employs the signal amplitude difference between T_2^* and T_1-T_2 spectra to obtain the SOM content. The second, Method II, directly quantifies the SOM signal from the T_1-T_2^* spectrum. A novel parameter, the ratio of T_1/T_2^* to T_1/T_2, is also proposed to refine the identification of SOM in the T_1-T_2 spectrum. The effectiveness of the proposed methods is validated by strong correlations with four geochemical parameters indicative of SOM content. The results from Method I show significantly improved correlations with all four geochemical parameters compared to the conventional T_1-T_2 method. The results from Method II show excellent correlations with parameters from step-by-step (SBS) Rock-Eval pyrolysis, reaching coefficients of determination (R^2) as high as 0.8958 and 0.8828. This method also shows strong numerical consistency with the geochemical parameters, specifically with (*6§jOñjtY•LiFFTueSGK*,

Currently, quantitative characterization of SOM in shale oil reservoirs predominantly relies on geochemical laboratory methods, particularly solvent extraction and Rock-Eval pyrolysis. The solvent extraction method is employed to separate soluble bitumen from SOM. The remaining extraction residue subsequently undergoes acid and base treatment to isolate the insoluble kerogen fraction. This sequential

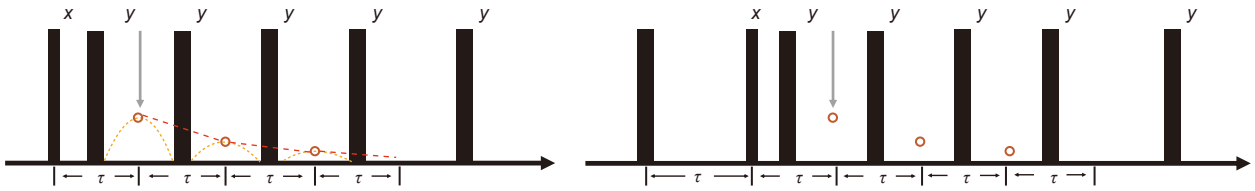

Fig. 1. Schematic diagrams of **(a)** CPMG, **(b)** FID, **(c)** IR-CPMG, and **(d)** IR-FID pulse sequences.

inhomogeneity of the magnetic field. In porous media like shale, significant field gradients are induced by the magnetic susceptibility difference, $\Delta\chi$, between pore fluids and the solid matrix (minerals and solid organic matter, SOM). This effect causes hydrogen in or near solid surfaces, particularly within SOM, to exhibit extremely short T_2^* values.

2.2. Pulse sequences

The ability to detect these ultra-short relaxation components is critically dependent on the pulse sequence's timing parameters. Conventional CPMG sequences are limited by a first TE that is typically between 60 and 100 μs for laboratory NMR instruments. This long initial delay prevents the detection of signals that decay faster than TE, leading to a significant underestimation of solid-like components such as SOM.

In contrast, the FID sequence offers a decisive advantage. Its instrument dead time (τ_d) can be as short as 20 μs or less, allowing it to capture the initial, rapidly decaying part of the signal that is completely missed by CPMG. This capability makes FID-based measurements uniquely suited for the direct characterization of SOM.

These measurements are combined within 2D experiments for comprehensive characterization. Through the integration of an IR pulse sequence, T_1-T_2 spectra are acquired with the IR-CPMG sequence, as shown in Fig. 1(c). T_1-T_2^* spectra are obtained using the IR-FID sequence as shown in Fig. 1(d). Since the T_1 encoding part of both sequences is identical, any difference in the resulting 2D spectra is directly attributable to the distinct between the T_2 and T_2^* transverse relaxation measurements. This fundamental distinction forms the basis of our novel methodology for identifying and quantifying SOM.

2.3. Identification of gaseous hydrocarbons using the $(T_1/T_2^*)/(T_1/T_2)$ ratio

When T_1-T_2 and T_1-T_2^* measurements are performed on the same shale sample with identical acquisition parameters during the T_1 recovery process, the NMR response of a specific hydrogen component in shale satisfies:

$$\frac{(T_1/T_2{}^*)}{(T_1/T_2)} \approx \frac{T_2}{T_2{}^*} = 1 + T_2\gamma(\Delta B_0 + \Delta\chi B_0) \tag{2}$$

Considering the influence of magnetic susceptibility differences $\Delta\chi$, Eq. (2) can be further expressed as:

$$\frac{(T_1/T_2{}^*)}{(T_1/T_2)} \approx 1 + T_2\gamma[\Delta B_0 + (\chi_H - \chi_m)B_0] \tag{3}$$

where χ_H represents the magnetic susceptibility of the hydrogen component, and χ_m denotes the magnetic susceptibility of the mineral matrix. The presence of strongly paramagnetic minerals, such as pyrite, within the matrix is the primary source of this contrast, creating a pervasive background magnetic field gradient throughout the porous medium.

Crucially, the T_2 term in Eq. (3) is the intrinsic transverse relaxation time, a property governed by the molecular mobility of a given hydrogen component. Different components in shale exhibit vastly different intrinsic T_2 values. For instance, SOM, with its rigidly bound protons, exhibits an extremely short intrinsic T_2 in the order of microseconds. Hydrocarbons with low mobility have a short T_2 in the low millisecond range. In contrast, hydrocarbons with high mobility such as light oils and gas possess long T_2 values, ranging from ones to hundreds of milliseconds.

Eq. (3) thus reveals the underlying physical mechanism whereby the $(T_1/T_2^*)/(T_1/T_2)$ ratio leverages a component's intrinsic T_2 values as an amplifier for the effect of the static gradient. The significant differences in the intrinsic T_2 values lead to a clear hierarchy in the resulting ratio. This relationship can be expressed as:

$$\frac{(T_1/T_2{}^*)}{(T_1/T_2)}_{\text{SOM}} \quad \frac{(T_1/T_2{}^*)}{(T_1/T_2)}_{\text{low-mobility}} = \frac{(T_1/T_2{}^*)}{(T_1/T_2)}_{\text{high-mobility/gas}} \tag{4}$$

where the subscripts represent different hydrogen components: the subscript “SOM” stands for solid organic matter, “low-mobility” for hydrocarbons with low mobility, “high-mobility” for hydrocarbons with high mobility, and “gas” for gaseous hydrocarbons.

This contrast provides a reliable basis for distinguishing between SOM and gaseous hydrocarbons, particularly within the conventional T_1-T_2 spectrum where the signal from gaseous hydrocarbons is fully captured.

2.4. Method I: SOM quantification based on T_2^* spectrum correction

Fig. 2 displays the T_1-T_2 spectrum for different hydrogen components in shale oil reservoirs. Peak A is generally considered to represent SOM. Peaks B, C, and D correspond to hydrocarbons with low mobility I, hydrocarbons with high mobility, and hydrocarbons with low mobility II, respectively. Peak E represents a mixed

fluid phase of hydrocarbons with high mobility and water. Peak F denotes free water, and Peak G indicates clay-bound water. Peak H, characterized by a high T_1 value and short T_2 response, can represent either SOM or gaseous hydrocarbons. The latter can be identified using the $(T_1/T_2^*)/(T_1/T_2)$ Ratio. An initial estimation of the SOM content in shale oil core samples can be obtained by integrating the signal amplitudes of Peak A, or both Peak A and Peak H, from the T_1-T_2 spectrum.

As established previously, this conventional estimation is inherently incomplete because T_1-T_2 measurements fail to detect the full signal from ultra-short relaxation components. Method I is proposed to addresses this deficiency by using the comprehensive signal from a T_2^* spectrum to correct the T_1-T_2 spectrum. This approach operates on the key assumption that the signal lost by the IR-CPMG sequence is entirely attributable to undetected SOM. Therefore, a corrected SOM signal amplitude is calculated by adding this signal deficit to the originally measured SOM amplitude as described by the following equation:

$$\phi_{\mathrm{OM,corr}} = \phi_{t,T_2{}^*} - \phi_{t,T_1-T_2} + \phi_{\mathrm{OM},T_1-T_2} \tag{5}$$

where $\phi_{\mathrm{OM,corr}}$ represents the SOM content obtained after correcting the T_1-T_2 spectrum, $\phi_{t,T_2{}^*}$ is the total hydrogen content derived from the T_2^* spectrum, ϕ_{t,T_1-T_2} is the total hydrogen content derived from the T_1-T_2 spectrum, and $\phi_{\mathrm{OM},T_1-T_2}$ is the SOM content obtained from the T_1-T_2 spectrum.

2.5. Method II: SOM identification and quantification via T_1-T_2^* spectrum

Fig. 3 presents the T_1-T_2^* spectrum for different hydrogen components in shale oil reservoirs. In this spectrum, the signal of SOM primarily appears in regions corresponding to peak A and peak H, and it is comprehensively captured by the IR-FID sequence. However, the SOM signal in the Peak H region is susceptible to interference from gaseous hydrocarbons due to the influence of magnetic field inhomogeneity.

This interference is eliminated through a systematic correction. The final SOM content $\phi_{\mathrm{OM},T_1-T_2{}^*}$ is calculated by subtracting the contribution of gaseous hydrocarbons from the total signal amplitude in the T_1-T_2^* spectrum, according to the following equation:

$$\phi_{\mathrm{OM},T_1-T_2{}^*} = A_{\mathrm{region},T_1-T_2{}^*} - A_{\mathrm{gas},T_1-T_2} \tag{6}$$

where $A_{\mathrm{region},T_1-T_2{}^*}$ represents the total signal amplitude integrated from the SOM region in the T_1-T_2^* spectrum, A_{gas,T_1-T_2} is the signal amplitude of gaseous hydrocarbons determined in T_1-T_2 spectrum.

3. Experimental

3.1. Materials

The Chang 7 Member of the Triassic Yanchang Formation in the Ordos Basin hosts a suite of organic-rich lacustrine black shales. These shales are characterized by exceptionally high organic matter abundance, moderate thermal maturity, and strong hydrocarbon generation potential, representing one of the primary source rock intervals in the Ordos Basin.

Table 1
Mineralogical composition of the representative shale samples determined by XRD analysis. Note: Q: Quartz; K: K-feldspar; PL: Plagioclase; C: Calcite; D: Dolomite; S: Siderite; PY: Pyrite; CM: Clay minerals; I/S: Illite/Smectite mixed-layer; I: Illite; K: Kaolinite; C: Chlorite.

Sample ID	Q, %	K, %	PL, %	C, %	D, %	S, %	PY, %	CM, %	I/S, %	I, %	K, %	C, %
#26	41.4	1.9	9.2	/	/	/	3.1	44.4	31	48	11	10
#28	31.6	4.2	9.8	/	2.7	/	3.4	48.3	52	32	8	8
#30	38.3	4.0	7.4	/	3.8	/	0.9	45.6	44	38	9	9
#31	37.8	1.3	1.9	/	1.0	/	4.6	53.4	34	50	10	6
#32	32.8	4.9	8.7	/	4.7	10.7	1.7	36.5	39	46	8	7
#34	31.9	13	7.7	/	2.1	/	/	45.3	49	36	8	7
#35	19.5	1.7	4.2	/	48.5	4.1	1.8	20.2	43	39	10	8
#36	32.4	3.6	5.9	/	1.9	7.8	1.5	46.9	/	83	9	8
#40	30.3	2.6	4.1	/	3.6	11.5	6.1	41.8	61	28	7	4
#43	26.8	3.1	5.6	/	3.2	4.8	10.9	45.6	46	34	10	10
#45	33.3	1.3	3.1	/	4.2	/	7.4	50.7	42	43	9	6
#50	45.6	3.7	4.6	/	/	/	5.0	41.1	26	52	12	10
#53	32.1	0.9	3.5	/	/	7	4.0	52.5	39	48	8	5
#58	41.5	0.9	3.8	/	0.9	3.7	0.5	48.7	27	63	5	5
#59	31.0	0.9	3.1	/	/	3.8	5.0	56.2	29	56	9	6
#61	40.2	2.1	6.4	/	/	7.2	7.3	36.8	33	43	12	12
#65	39.4	0.8	3.5		7.2	5.9	2.8	40.4	33	58	4	5
#127	29.2	5.7	12.6	/	/	/	1.4	51.1	59	26	6	9
#128	37.9	3.7	13.1		/	/	1.6	43.7	52	28	6	14
#129	40.7	4.3	12.8	2.9	/	/	1.8	37.5	50	27	6	17

resonance frequency of $_0/2\pi = f_0 = 21.36$ MHz and is equipped with a 25 mm probe. All measurements were performed at a room temperature of approximately 25 °C.

(1) FID measurements

The FID measurements were conducted using the following acquisition parameters: a repetition time TW of 10 s, an instrument dead time τ_d of 17 μs, a data sampling interval τ_2 of 1 μs, and 983 acquisition points. Sufficient signal averaging was performed for each experiment, to ensure a signal-to-noise ratio (SNR) greater than 100.

The acquired FID data were processed using an inversion algorithm developed by the research team to obtain the T_2^* spectra. The inversion results were calibrated using a standard water sample and converted into equivalent water content per unit mass (in mg/g), allowing quantitative comparison with geochemical results.

(2) IR-CPMG and IR-FID measurements

In the IR-CPMG measurements, the inversion recovery delay time τ_3 in the T_1 recovery period was varied logarithmically from 58 μs to 10 s, with 28 different τ_3 values. In the T_2 decay period, the echo spacing (TE = $2\tau_1$) was set to 0.1 ms, and 300 echoes were acquired. The T_1 recovery period in IR-FID measurements used the same τ_3 values as the IR-CPMG measurements. The T_2^* decay phase followed the same parameters as the one-dimensional FID measurements: $\tau_d = 17$ μs, $\tau_2 = 1$ μs, and 983 data points.

Both IR-CPMG and IR-FID measurements involved a sufficient number of signal accumulations to ensure an overall average SNR greater than 100. The acquired 2D data were subjected to inversion processing to yield T_1-T_2 spectra and T_1-T_2^* spectra, respectively. The signal amplitudes of both types of 2D spectra were calibrated using a standard water sample and converted to equivalent water content per unit mass of the sample, in mg/g.

3.3. Geochemical analysis

(1) TOC content analysis

TOC content was measured using a CS-i carbon–sulfur analyzer, following the GB/T19145-2003 standard. TOC reflects the total amount of organic carbon in the sample, including carbon present in hydrocarbons, bitumen, and kerogen. It is one of the commonly used indicators for evaluating organic matter abundance.

(2) Routine Rock-Eval pyrolysis

Routine Rock-Eval pyrolysis experiments were conducted using a Rock-Eval 6 instrument. Powder samples were first heated isothermally at 300 °C for 3 min to obtain the S_1 peak. The temperature was then ramped up to 650 °C at a rate of 25 °C/min to obtain the S_2 peak. Hydrocarbons released during the pyrolysis process were detected by a flame ionization detector and quantified based on calibration with a standard sample. The S_1 peak typically represents the content of free hydrocarbons, and the S_2 peak corresponds to the amount of cracking hydrocarbons generated from the thermal decomposition of heavy hydrocarbons, bitumen, and kerogen. The S_2 peak is a key geochemical indicator used to assess hydrocarbon generation potential and organic matter richness.

(3) Step-by-step (SBS) Rock-Eval pyrolysis

SBS Rock-Eval pyrolysis was also performed using a Rock-Eval 6 instrument. The detailed heating program was as follows. The sample was initially heated from 120 to 200 °C at a rate of 25 °C per minute and held at 200 °C for 3 min to obtain the $S_{1\text{-}1}$ peak. The temperature was then increased to 300 °C at the same heating rate and maintained for 3 min to acquire the $S_{1\text{-}2a}$ peak. Subsequently, the temperature was raised to 350 °C and held for 3 min to obtain the $S_{1\text{-}2b}$ peak. The heating continued to 450 °C, where the sample was again held for 3 min to generate the $S_{2\text{-}1}$ peak. Finally, the temperature was increased to 600 °C and maintained for 3 min to obtain the $S_{2\text{-}2}$ peak.

Fig. 4 illustrates the geochemical significance of the products released at different temperature stages during the SBS Rock-Eval experiment. A better understanding of the compositional characteristics of these fractionated pyrolysis products can be achieved by comparing their elution temperatures with the boiling points of *n*-alkanes within corresponding carbon number ranges.

The $S_{1\text{-}1}$ peak primarily represents light molecular weight oil components with carbon numbers of 11 or less, such as *n*-undecane (*n*-$C_{11}H_{24}$), which has a boiling point of 196 °C. The subsequent $S_{1\text{-}2}$ peak represents light to medium molecular weight oil fractions and is further divided into the $S_{1\text{-}2a}$ and $S_{1\text{-}2b}$ sub-peaks. The $S_{1\text{-}2a}$ peak, observed between 200 and 300 °C, corresponds to compounds with carbon numbers ranging from 12 to 17, exemplified by *n*-heptadecane (*n*-$C_{17}H_{36}$), which boils at 302 °C. The $S_{1\text{-}2b}$ peak, appearing between 300 and 350 °C, is associated with compounds having carbon numbers between 18 and 20, such as *n*-eicosane (*n*-$C_{20}H_{42}$), with a boiling point of 342.7 °C. The $S_{2\text{-}1}$ peak, generated between 350 and 450 °C, mainly reflects heavier hydrocarbons and asphaltenes with carbon numbers in the range of 21–30. A typical example is *n*-triacontane (*n*-$C_{30}H_{62}$), which has a boiling point of 449.8 °C. Finally, the $S_{2\text{-}2}$ peak, formed between 450 and 600 °C, primarily indicates the thermal degradation products of kerogen. Some studies classify the $S_{1\text{-}1}$, $S_{1\text{-}2a}$, and $S_{1\text{-}2b}$ peaks as representing free hydrocarbons, the $S_{2\text{-}1}$ peak as adsorption hydrocarbons, and the $S_{2\text{-}2}$ peak as cracking hydrocarbons (Jiang et al., 2016; Zhang et al., 2020; Li et al., 2020).

Therefore, the parameter ($S_{2\text{-}1}$+$S_{2\text{-}2}$) represents the total amount of hydrocarbons generated from the thermal cracking of heavy hydrocarbons, bitumen, and kerogen. Its geochemical significance is consistent with the S_2 peak from routine Rock-Eval pyrolysis. However, the results obtained through step-by-step heating are less affected by the pyrolysis carry-over and confinement effect, leading to more precise outcomes. It is important to note the physical states of normal alkanes at the NMR measurement temperature (approximately 25 °C), considering that the NMR measurements in this study were conducted at this room temperature. Normal alkanes with carbon numbers of 17 or less, such as *n*-heptadecane (*n*-$C_{17}H_{36}$), are liquid at 25 °C, as its melting point is around 21 °C. In contrast, those with carbon numbers of 18 or greater, such as *n*-octadecane (*n*-$C_{18}H_{38}$), are solid, with melting points ranging from approximately 28 to 30 °C. Consequently, the parameter ($S_{1\text{-}2b}$ + $S_{2\text{-}1}$+$S_{2\text{-}2}$) signifies the total content of solid petroleum hydrocarbons, bitumen, and kerogen in the sample at NMR measurement temperature. This sum represents the total content of hydrocarbons existing in a solid state within the sample and can also serve as a key geochemical indicator for characterizing the SOM content of the sample.

4. Results and discussion

4.1. NMR measurements results

To illustrate the typical NMR responses observed across the sample set, the T_1-T_2 and T_1-T_2^* spectra of three representative shale samples (#45, #34 and #35), selected for their high, medium, and low SOM content, are shown in Fig. 5. The spectral peak regions were delineated in both spectra according to the distribution characteristics of each peak in Figs. 2 and 3. It can be observed that the T_1-T_2 and T_1-T_2^* spectra of the same sample exhibit consistent peak positions, with similar T_1 relaxation responses for peaks bearing the same labels. The primary differences lie in the transverse relaxation responses (T_2 and T_2^*). The T_2^* values of all hydrogen-bearing components are

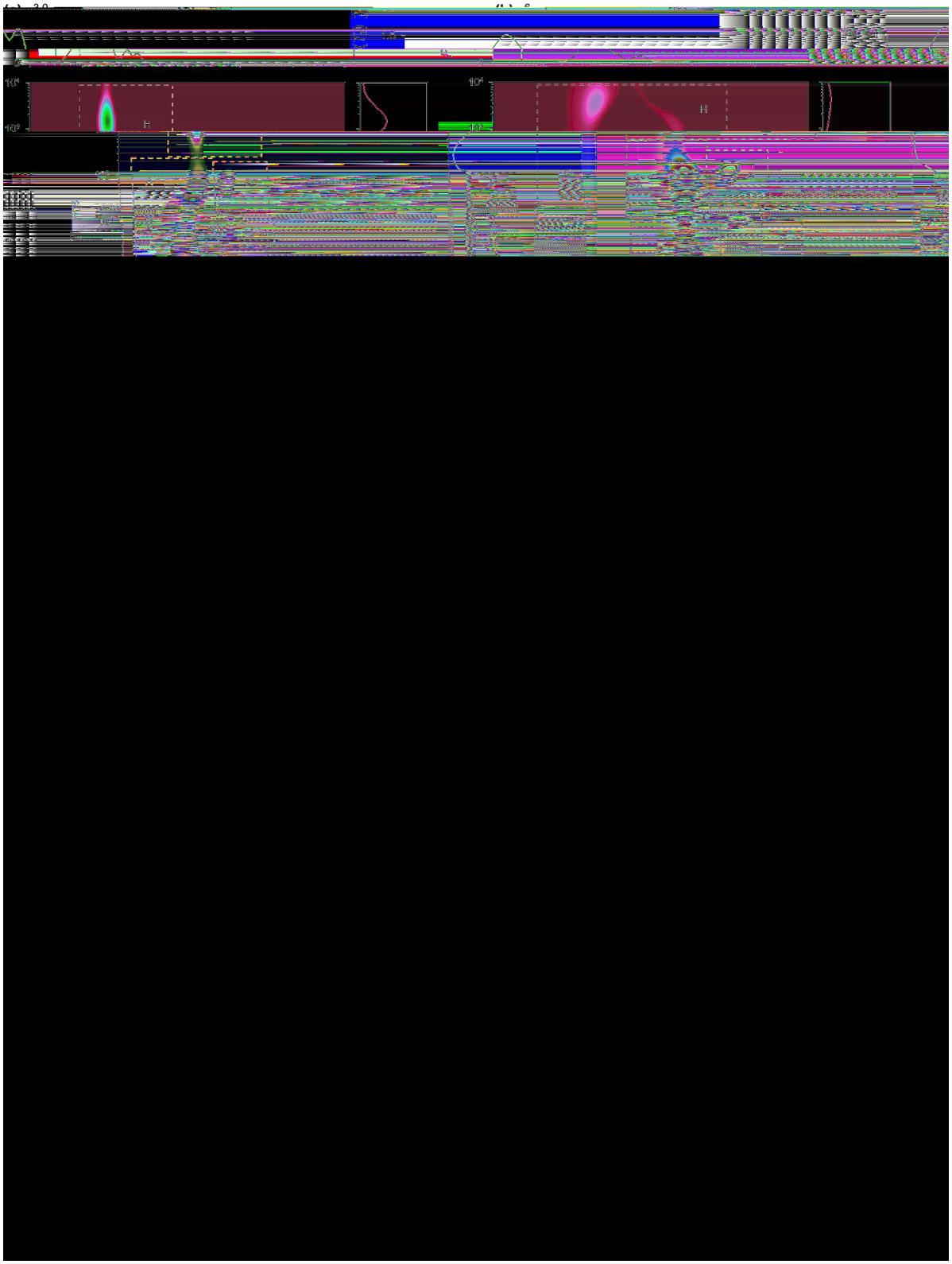

Fig. 5. Comparison of conventional T_1-T_2 spectra and the corresponding T_1-T_2^* spectra for three representative shale samples with high, medium, and low SOM content. The paired plots are for samples: **(a)** & **(b)** #45; **(c)** & **(d)** #34; **(e)** & **(f)** #35. For each pair, the left part is the T_1-T_2 spectrum and the right part is the T_1-T_2^* spectrum.

addition, heavy hydrocarbons, bitumen, and kerogen (S_2) account for a substantial proportion of the total hydrocarbon content (S_1+S_2), ranging from 50.86% to 86.41%. The T_{max} values range from 430 to 449 °C, indicating a moderate level of thermal maturity. As indicated in Table 2, all samples fall within the early oil window stage.

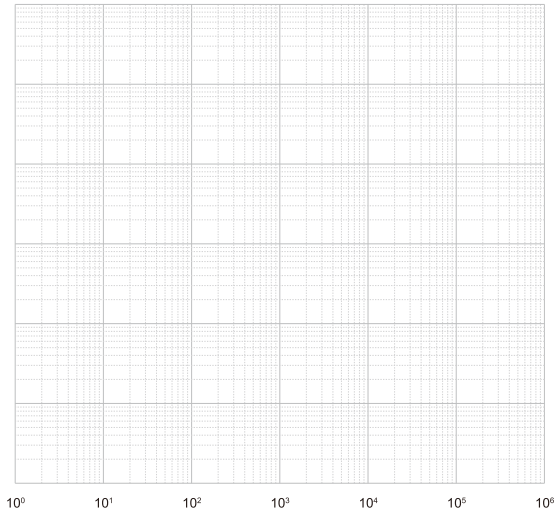

Fig. 6. Distribution of $(T_1/T_2^*)/(T_1/T_2)$ ratio for different hydrogen component peaks in shale samples.

Table 3
TOC contents analysis and routine Rock-Eval pyrolysis results for shale samples.

Sample ID	TOC, wt%	S_1, mg/g	S_2, mg/g	T_{max}, °C
#26	3.63	2.74	10.51	439
#28	4.49	3.67	10.24	442
#30	3.90	2.87	8.61	444
#31	4.40	3.37	9.86	441
#32	4.91	3.74	12.67	441
#34	3.81	3.29	9.09	447
#35	0.64	1.14	1.18	436
#36	5.50	3.26	14.21	446
#40	5.23	2.77	12.00	443
#43	4.50	2.84	9.36	445
#45	6.38	3.65	15.24	439
#50	5.44	2.98	15.31	443
#53	4.23	4.37	12.63	430
#58	4.44	3.95	13.98	440
#59	7.11	3.73	23.72	440
#61	5.24	4.00	14.84	445
#65	3.99	4.48	12.87	435
#127	4.78	3.87	15.22	449
#128	4.55	5.17	17.71	443
#129	4.09	3.84	13.95	447

Table 2
Solid organic matter (SOM) content calculated results based on method I and II for shale samples.

Sample ID	ϕ_{t,T_2^*}, mg/g	ϕ_{t,T_1-T_2}, mg/g	ϕ_{OM,T_1-T_2}, mg/g	$\phi_{OM,corr}$, mg/g	$\phi_{OM,T_1-T_2^*}$, mg/g
#26	46.07	26.72	8.21	27.56	13.60
#28	40.58	24.16	8.76	25.18	11.05
#30	48.24	28.66	11.07	30.65	11.62
#31	36.49	21.29	7.01	22.20	15.36
#32	42.80	23.02	8.34	28.12	16.21
#34	31.44	23.95	8.35	15.85	11.11
#35	20.04	15.66	3.09	7.47	3.95
#36	62.67	23.74	9.14	48.07	21.40
#40	48.44	21.47	8.37	35.33	14.87
#43	37.13	21.07	7.40	23.46	13.90
#45	67.03	22.68	8.47	52.82	21.53
#50	55.80	27.97	9.68	37.51	17.64
#53	50.73	27.28	5.40	28.85	14.36
#58	53.84	25.95	5.91	33.80	14.58
#59	59.99	27.47	7.77	40.29	23.42
#61	45.63	20.07	6.44	32.00	15.58
#65	39.84	25.75	4.74	18.82	14.47
#127	66.75	37.71	7.89	36.94	16.23
#128	48.86	38.18	11.52	22.19	11.95
#129	45.16	39.86	9.56	14.86	10.47

The SBS Rock-Eval pyrolysis analysis results for these shale samples are detailed in Table 4. Compared to routine Rock-Eval pyrolysis, the S_1 content ($S_{1\text{-}1}$+$S_{1\text{-}2a}$ + $S_{1\text{-}2b}$) obtained from SBS Rock-Eval pyrolysis ranges from 2.89 to 8.05 mg/g, approximately 1.13–2.53 times higher than conventional S_1 values. The S_2 content ($S_{2\text{-}1}$ + $S_{2\text{-}2}$) derived from this method ranges from 1.42 to 20.67 mg/g, comparable to S_2 values obtained through routine Rock-Eval pyrolysis. The cracking hydrocarbons ($S_{2\text{-}1}S_{2\text{-}2}$) accounts for approximately 32.95%–81.18% of the total hydrocarbon content ($S_{1\text{-}1}$+$S_{1\text{-}2a}$ + $S_{1\text{-}2b}$ + $S_{2\text{-}1}$ +$S_{2\text{-}2}$). The ($S_{1\text{-}2b}$ + $S_{2\text{-}1}$+$S_{2\text{-}2}$) content for these samples ranges from 1.94 to 21.94 mg/g, constituting approximately 45.01%–84.09% of the total hydrocarbon content. These findings suggest that hydrocarbons in the analyzed shale samples exist predominantly in a solid state under NMR experimental conditions.

4.3. Correlation analysis between NMR measurements and geochemical parameters

The correlation between the three SOM quantification methods and selected geochemical parameters is analyzed based on the previously discussed NMR measurements and geochemical data. Three methods are included in this analysis. The first is Method I (Method I: T_1-T_2&T_2^*), which is based on the T_1-T_2 spectrum and T_2^* spectrum difference correction. The second is Method II (Method II: T_1-T_2^*), which is based on the T_1-T_2^* spectrum. The third is the conventional method (Method: T_1-T_2) based on the T_1-T_2 spectrum. Four geochemical parameters capable of reflecting SOM content were selected for the correlation analysis: TOC, S_2 from routine Rock-Eval pyrolysis, ($S_{2\text{-}1}$+$S_{2\text{-}2}$) and ($S_{1\text{-}2b}$ + $S_{2\text{-}1}$+$S_{2\text{-}2}$) from SBS Rock-Eval pyrolysis. The quantitative accuracy of each method is

Table 4
Step-by-step (SBS) Rock-Eval pyrolysis results for shale samples. Note: The S_1 and S_2 values are calculated as $S_1 = S_{1\text{-}1} + S_{1\text{-}2a} + S_{1\text{-}2b}$ and $S_2 = S_{2\text{-}1} + S_{2\text{-}2}$.

Sample ID	$S_{1\text{-}1}$, mg/g	$S_{1\text{-}2a}$, mg/g	$S_{1\text{-}2b}$, mg/g	$S_{2\text{-}1}$, mg/g	$S_{2\text{-}2}$, mg/g	S_1, mg/g	S_2, mg/g	$S_2+S_{1\text{-}2b}$, mg/g
#26	2.01	1.97	0.99	7.20	5.36	4.97	12.56	13.55
#28	2.59							

visually compared in the crossplots of Fig. 7(b)–(d), where the diagonal line represents a perfect agreement between the NMR-derived and Rock-Eval values.

The conventional T_1-T_2 method exhibits the weakest correlation with the four geochemical parameters. As shown in the figures, the gray circles are all located above the diagonal line, which confirms the fact that this method struggles to effectively capture signals from ultra-short relaxation components, leading to an underestimation of SOM content.

In comparison to the conventional T_1-T_2 method, the results from Method I show significantly improved correlations with all four geochemical parameters. It demonstrates great correlations with ($S_{2\text{-}1}$+$S_{2\text{-}2}$) and ($S_{1\text{-}2b} + S_{2\text{-}1}$+$S_{2\text{-}2}$), achieving high coefficients of determination (R^2) of 0.7176 and 0.6956 respectively. However, as illustrated in Fig. 7(b)–(d), the green data points for this method are all located below the diagonal line, indicating that the SOM values calculated by this method are systematically higher than the Rock Eval pyrolysis values. However, a key limitation of this method is its inability to distinguish the origin of these signals. Consequently, some liquid hydrocarbons with low-mobility and gaseous hydrocarbons are also counted in the SOM content, leading to an overestimation. This non-selective detection is precisely why Method I correlates so well with the S_2 parameter, as its content is also known to include these components.

The results from Method II also show markedly improved correlations with the four geochemical parameters compared to the other methods. It achieves a particularly high R^2 of 0.8828 with ($S_{1\text{-}2b} + S_{2\text{-}1}$+$S_{2\text{-}2}$) and the highest overall correlation with ($S_{2\text{-}1}$+$S_{2\text{-}2}$), reaching an R^2 of 0.8958. As shown in Fig. 7(b)–(d), the corresponding yellow circles for this method are distributed near the diagonal line. This indicates that the SOM content obtained by this method is more consistent with the Rock-Eval results than the other two methods. This improved consistency is attributed to the mitigation of the overestimation issue inherent in Method I. It effectively excludes interference from liquid or gaseous hydrocarbon components by using T_1-dimensional information and a gas correction.

It can also be observed that the data for S_2 and ($S_{2\text{-}1}$+$S_{2\text{-}2}$) are systematically positioned below the diagonal line, although they are proximate to the diagonal line. This indicates that a slight overestimation by Method II relative to these parameters. In contrast, the data points for the ($S_{1\text{-}2b} + S_{2\text{-}1}$+$S_{2\text{-}2}$) parameter show excellent consistency. Most values fall directly on the diagonal. This excellent consistency indicates that the results obtained from Method II include the $S_{1\text{-}2b}$ component, which are medium molecular weight hydrocarbon fractions. These hydrocarbon fractions exist in a solid state at the NMR measurement temperature. Therefore, it is concluded that this method accurately quantifies the total sum of solid hydrogen components, including solid petroleum hydrocarbons, bitumen, and kerogen.

In conclusion, the two new methods proposed in this paper significantly improve the quantitative characterization of SOM. Method I provides a rapid estimation of total content of SOM but is prone to overestimation by including signals from liquid or gaseous hydrocarbon components. Method II successfully corrects for these interferences, accurately quantifying the total solid hydrogen content with results highly consistent with advanced Rock-Eval pyrolysis. Furthermore, both the proposed NMR-based methods offer clear practical advantages over the TOC content analysis and Rock-Eval pyrolysis. They are non-destructive, increase the sample volume nearly 600-fold from approximately 100 mg of powder to 60 g of core plug for enhanced representativeness, and eliminate complex, time-consuming procedures.

4.4. Discussion

This section discusses the applicability and limitations of the proposed methodology by examining the influence of two key factors pertinent to geological reservoirs: magnetic field inhomogeneity and temperature.

Magnetic field inhomogeneity is a critical factor for the NMR T_2^* relaxation analysis of shales. A primary source of such inhomogeneity in shales is the presence of paramagnetic minerals. The samples in this study contain pyrite, as shown in Table 1, which is a primary source of internal magnetic field gradients causing the signal of nearby hydrogen nuclei to decay rapidly. FID-based T_2^* measurements acquire data immediately following the instrument dead time, allowing for the characterization of such fast-relaxing signals. The strong consistency (Fig. 7(d)) demonstrates that the T_2^* measurement is effective for the shales in this study, which contain pyrite content up to 10.9 %. Furthermore, recent numerical simulations (Liu et al., 2025) also indicate that pyrite contents in the range of 1.51%–5.43% have a limited impact on the quantification of the SOM's T_2^* response. However, the FID

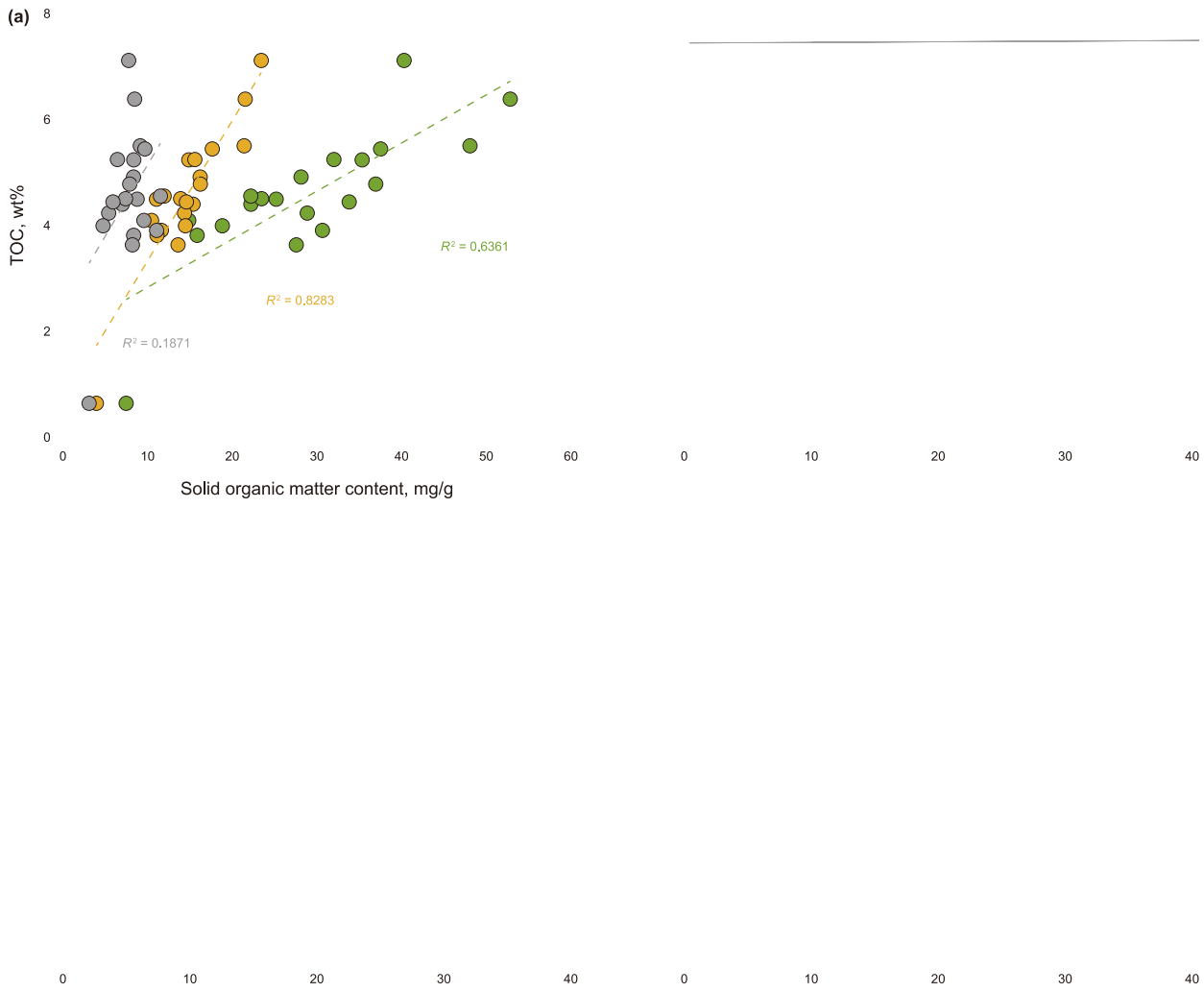

Fig. 7. Correlation analysis between organic matter content calculated by different NMR methods and geochemical parameters. The plots show correlations with **(a)** TOC, **(b)** the routine Rock-Eval pyrolysis parameter S_2, the sum of SBS pyrolysis parameters **(c)** $S_{2\text{-}1} + S_{2\text{-}2}$, and **(d)** $S_{1\text{-}2} + S_{2\text{-}1} + S_{2\text{-}2}$.

measurements signal decay could become too rapid to be fully captured for shales with exceptionally high magnetic field inhomogeneity, which would potentially lead to an underestimation of SOM and pore fluid.

The NMR measurements in this work were conducted at an ambient temperature of 25 °C. The physical state of various hydrocarbon fractions aligns with the classification criteria for the geochemical parameter ($S_{1\text{-}2b} + S_{2\text{-}1}+S_{2\text{-}2}$) at this temperature, which quantifies the solid hydrocarbon fraction under surface conditions. This allows for a direct comparison between the NMR-detected solid hydrogen signal and a geochemically defined solid hydrocarbon mass. It is well-established that increased molecular mobility leads to longer intrinsic T_1 and T_2 values at reservoir temperatures. This causes NMR signals to shift from a solid-like response (T_2 T_1) towards a more liquid-like response ($T_1 \propto T_2$), a behavior that has been experimentally documented in analogous heavy hydrocarbon systems (Serve et al., 2021). Consequently, the SOM content quantified at 25 °C represents the total solid hydrocarbon resource at the surface, a portion of which transitions to a mobile liquid phase at reservoir conditions. However, the influence of temperature is different for T_2^* relaxation in shale. The T_2^* relaxation rate is the sum of the temperature-dependent intrinsic relaxation rate ($1/T_2$) and the temperature-independent contribution from magnetic field inhomogeneity. The T_2^* response is primarily controlled by magnetic field inhomogeneity for shale under the measurement conditions of this study. Consequently, the overall T_2^* relaxation is demonstrated to be remarkably insensitive to temperature changes, as the dominant contribution from magnetic field inhomogeneity is temperature-invariant. This inherent stability suggests that FID-based quantification methods are likely to be significantly more robust against temperature variations than conventional T_2-based measurements, representing a significant potential advantage for evaluating shale resources under diverse thermal regimes.

5. Conclusions

In this paper, FID and IR-FID pulse sequences were introduced to successfully address the limitations of conventional NMR measurements in shale oil reservoirs. Two novel methods are proposed for the quantitative characterization of SOM in shale reservoirs. The effectiveness of the proposed methods is systematically validated through a comparative analysis of the NMR-

Zhang, H., Huang, H., Li, Z., et al., 2020. Comparative study between sequential solvent-extraction and multiple isothermal stages pyrolysis: a case study on Eocene Shahejie formation shales, Dongying depression, East China. Fuel 263, 116591. https://doi.org/10.1016/j.fuel.2019.116591.

Zhao, W., Hu, S., Hou, L., et al., 2020. Types and resource potential of continental shale oil in China and its boundary with tight oil. Petrol Explor Dev+. 47 (1), 1–11. https://doi.org/10.1016/S1876-3804(20)60001-5.

Zhao, W., Bian, C., Li, Y., et al., 2023. Organic matter transformation ratio, hydrocarbon expulsion efficiency and shale oil enrichment type in Chang 7_3 shale of Upper Triassic Yanchang Formation in Ordos Basin, NW China. Petrol Explor Dev+. 50 (1), 14–26. https://doi.org/10.11698/PED.20220459.

Zou, C., Yang, Z., Cui, J., et al., 2013. Formation mechanism, geological characteristics and development strategy of nonmarine shale oil in China. Petrol Explor Dev+ 40 (1), 15–27. https://doi.org/10.1016/S1876-3804(13)60002-6.

Zou, C., Pan, S., Jing, Z., et al., 2020. Shale oil and gas revolution and its impact. Acta Pet. Sin. 41 (1), 1–12. https://doi.org/10.7623/syxb202001001.

Zou, C., Ma, F., Pan, S., et al., 2023. Formation and distribution potential of global shale oil and the developments of continental shale oil theory and technology in China. Earth Sci. Front. 30 (1), 128–142. https://doi.org/10.13745/j.esf.sf.2022.8.29.